Dynamics of the Acetylcholinesterase Tetramer

Alemayehu A. Gorfe,*† Chia-en A. Chang,*† Ivaylo Ivanov,*† and J. Andrew McCammon*†‡§
*Department of Chemistry and Biochemistry, †Center for Theoretical Biological Physics, ‡Howard Hughes Medical Institute, and §Department of Pharmacology, University of California at San Diego, La Jolla, California 92093-0365

ABSTRACT Acetylcholinesterase rapidly hydrolyzes the neurotransmitter acetylcholine in cholinergic synapses, including the neuromuscular junction. The tetramer is the most important functional form of the enzyme. Two low-resolution crystal structures have been solved. One is compact with two of its four peripheral anionic sites (PAS) sterically blocked by complementary subunits. The other is a loose tetramer with all four subunits accessible to solvent. These structures lacked the C-terminal amphipathic t-peptide (WAT domain) that interacts with the proline-rich attachment domain (PRAD). A complete tetramer model (AChEt) was built based on the structure of the PRAD/WAT complex and the compact tetramer. Normal mode analysis suggested that AChEt could exist in several conformations with subunits fluctuating relative to one another. Here, a multiscale simulation involving all-atom molecular dynamics and Cα-based coarse-grained Brownian dynamics simulations was carried out to investigate the large-scale intersubunit dynamics in AChEt. We sampled the ns-μs timescale motions and found that the tetramer indeed constitutes a dynamic assembly of monomers. The intersubunit fluctuation is correlated with the occlusion of the PAS. Such motions of the subunits "gate" ligand-protein association. The gates are open more than 80% of the time on average, which suggests a small reduction in ligand-protein binding. Despite the limitations in the starting model and approximations inherent in coarse graining, these results are consistent with experiments which suggest that binding of a substrate to the PAS is only somewhat hindered by the association of the subunits.

INTRODUCTION

Termination of nerve impulses in cholinergic synapses requires very rapid hydrolysis of the neurotransmitter acetylcholine (ACh). This is carried out by one of the most efficient enzymes known—acetylcholinesterase (AChE) (1). AChE is found in all vertebrates and invertebrates so far investigated, as well as in other species (2). Structurally, AChE belongs to the α/β hydrolase protein fold and has been purified and crystallized in the monomeric, dimeric, and tetrameric forms (3,4).

The tetramer is the most important functional form of the enzyme under physiological conditions. The crystal structure of recombinant mouse tetramer (mAChE) was solved at a resolution of 2.9 Å (5). The structure was characterized by an antiparallel alignment of two canonical homodimers with a compact, pseudosquare planar arrangement of the subunits. Furthermore, the soluble, trypsin-released tetrameric form of AChE from *Electrophorus electricus* (eAChE) was crystallized in two distinct crystal forms (6). The two low-resolution eAChE tetrameric structures, resolved to 4.5 and 4.2 Å, significantly differ in the arrangement of the catalytic domains: one is compact square nonplanar (Protein Data Bank (pdb) code 1C2O), whereas the other is loose, pseudosquare planar (pdb code 1C2B). It has therefore been suggested that the tetramer is flexible and could exist in multiple conformations separated by low barriers (5,6). Computations on the diffusion of ACh to the active sites of the tetrameric enzyme showed that the reaction rates differ for individual active sites in the compact structure (7,8). The rates are similar for individual active sites in the loose structure and an intermediate structure obtained by morphing between the two. The key findings of these studies were i), active sites are partially occluded in the compact structure with a competition for substrate between individual active sites, and ii), electrostatic forces substantially enhance the rate in the tetramer relative to the monomer.

The C-terminal ~40-residue t-peptide (9,10), also called the tryptophan amphiphilic tetramerization (WAT) domain, interacts with the proline-rich attachment domain (PRAD) of the collagen-like Q subunit (ColQ). ColQ is a structural protein that anchors AChE to the synaptic basal lamina. However, the mAChE tetramer entirely lacked the WAT domain, which was flexible and not observed in either of the eAChE structures. The t-peptide has a series of aromatic amino acids, including three equally spaced tryptophan residues (WWW). The crystal structure of the PRAD/WAT complex was solved at a resolution of 2.35 Å and showed a tight association through hydrogen bonding and hydrophobic interactions between the WWW motifs in WAT and consecutive proline residues in PRAD (11). Based on the crystal structures of the compact eAChE (pdb 1C2O) and the PRAD/WAT complex (pdb 1VZJ), Zhang and McCammon

Submitted July 20, 2007, and accepted for publication September 14, 2007.

Alemayehu A. Gorfe and Chia-en A. Chang contributed equally to this work.

Address reprint requests to Alemayehu A. Gorfe, Tel.: 858-822-0255; E-mail: abebe@mccammon.ucsd.edu; or Chia-en A. Chang, Tel.: 858-822-1469; E-mail: cchang@mccammon.ucsd.edu.

Editor: Gregory A. Voth.

0006-3495/08/02/1144/11 $2.00

doi: 10.1529/biophysj.107.117879

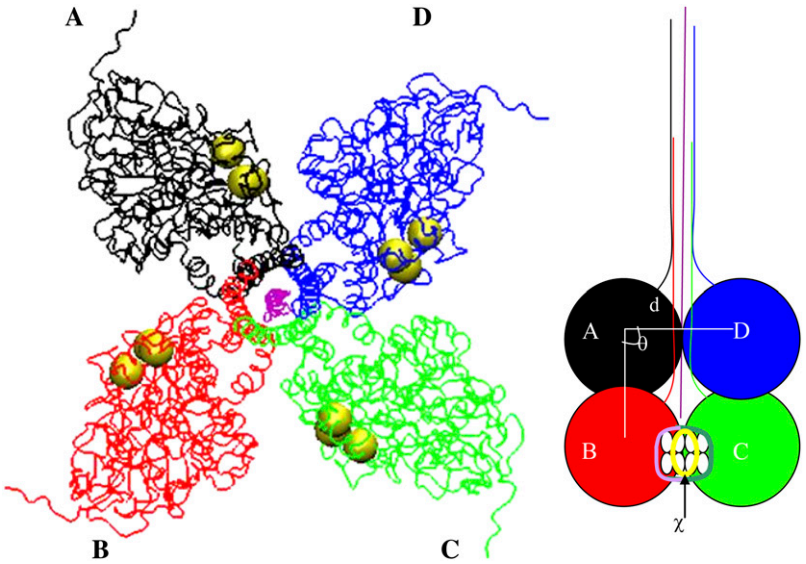

FIGURE 1 Model-built AChEt structure (*left*) and its schematic representation (*right*) showing subunits A (*black*), B (*red*), C (*green*), and D (*blue*). The ColQ onto which the WAT domains (residues 544–583) wrap around is in purple. Note the nearly symmetric arrangement of the monomers in this model. The three PAS residues (Tyr^{72}, Trp^{286}, and Tyr^{341}) are shown in yellow vdW spheres. The distances (d) between centers of subunits, the angle (θ) formed by three centers of subunits, and interfacial contact (χ) are illustrated. Note that χ represents the intersection (*yellow sphere*) of two selections: the numbers of atoms in one subunit that are within 10 Å of any atom in a complementary subunit and vice versa (see *green* and *lavender arcs*).

constructed a complete, roughly symmetric model of the complex of AChE tetramer (AChEt, Fig. 1) with the anchoring protein tail (12). Using block normal mode (BNM) analysis, they found several low-frequency and low-barrier normal modes corresponding to intersubunit motions due to the presence of flexible hinges. This flexibility may play a role in the near diffusion controlled breakdown of ACh (13,14).

To what extent does intersubunit fluctuation modulate catalytic efficiency? The answer to this question lies in being able to exhaustively sample the conformational space accessible to AChEt. Once the dominant configurations, i.e., the most populated ''low energy'' states, are identified, it will be possible to compute the probability of active site occlusion due to a complementary subunit and to correlate these structural features to function by, for example, calculating the reaction rates based on structures representing various conformational states. In principle, rigorous conformational sampling can be performed by atomistic molecular dynamics (MD) simulations. However, for a system with the complexity and size of AChEt, exhaustive sampling by atomistic, explicit water simulations is impractical; the low frequency and large amplitude intersubunit fluctuations cannot be sufficiently sampled in the few tens of nanoseconds generally afforded by fine-grained MD. Moreover, the high-frequency motions, which take up the major portion of atomistic simulation time, contribute very little to the large-scale intersubunit fluctuations. Therefore, less detailed but fast and inexpensive approaches are needed. On the other hand, access to the active center can also be modulated by local conformational changes in a complementary subunit. These motions may not be captured by the coarse-grained (CG) model. There is also the need to validate and parameterize the CG model. Thus, a multiscale simulation approach was adopted. In multiscale simulations, fine-grained models, such as atomistic MD, are combined with CG ones, such as Cα-based bead models. CG models, both alone and as part of a multiscale simulation scheme, are becoming increasingly useful to investigate large-scale molecular motions (15–21), such as those of AChEt.

In this work, we present results from multiscale simulations designed to explore the intersubunit motions. We combine all-atom MD (AA-MD) and CG Brownian dynamics (CG-BD) (22) simulations to characterize conformational states that AChEt may adopt at physiological conditions. The results show that there is indeed a substantial intersubunit movement (translational and rotational) that allows dynamic exposure of the active site in each subunit, albeit to various degrees. We also performed BNM analysis on selected snapshots from the AA-MD simulation and found three groups of principal modes, each composed of three modes representing closely related motions. Similar results were obtained from a principal component analysis (PCA) carried out on the CG-BD simulated structures.

METHODS

The model-built tetrameric AChE structure (AChEt, Fig. 1) was used as a starting point for the simulations after the following modifications. Since they do not contribute to structural stability but would increase system size, the first nine residues of ColQ were omitted. Note that ColQ has 47 residues, whereas each of the four AChE monomers is 583 amino acids long, with residues 544–583 constituting the WAT domain. We introduced physiologically existing disulfide bridges that connect i), the WAT of subunits A and B at residue 580, ii), ColQ and subunit C (residues 15 and 580), and iii), ColQ and subunit D (residues 16 and 580).

Classical molecular dynamics simulation

A 20 ns explicit water AA-MD simulation was performed. The total number of atoms in the simulation was ~256,000. Standard simulation procedures (e.g., (23)) were followed using the program NAMD (24) and the CHARMM22 force field (25). Briefly, after preparation of the system by sequential steps of

energy minimization and equilibration, the production phase was carried out at constant temperature (310 K) and pressure (1 atm) conditions. Periodic boundary conditions with full particle mesh Ewald electrostatics, a 10 Å cutoff for the van der Waals (vdW) interactions, a 12 Å cutoff for nonbonded list update, the SHAKE algorithm, and RESPA multiple time stepping (with 2, 1, 2 fs) were used.

Coarse-grained model and force field

CG model was also used to represent AChEt, where each residue is represented by a single interaction center (bead) placed on the α carbon. A charged residue was assigned $\pm$1e charge, and the beads were stepped through time by Brownian dynamics (BD) simulations. The force field parameters were based on those developed by Tozinni and McCammon (22,26), which were implemented in the UHBD simulation package (27,28). The force field has the functional form:

$$U = U_{\text{bond}} + U_{\text{angle}} + U_{\text{dihedral}} + U_{\text{vdw}} + U_{\text{elec}}. \qquad (1)$$

The bond and dihedral interactions are harmonic. The angle term is of quartic form, which allows transitions between two minima formed by an α-helix or a β-sheet. The vdW interactions, U_{vdw}, use a Morse potential as their functional form, where the equilibrium values are taken from a reference conformation (see Supplemental Material). The electrostatic interaction between each pair of beads i and j is $U_{\text{elec}} = q_i q_j/\varepsilon r_{ij}$, where r_{ij} is the distance between beads i and j. No detailed solvent model was used, but a distance-dependent dielectric constant ($\varepsilon_{ij} = 4r_{ij}$) was employed to avoid unrealistic in vacuo Coulombic interactions. The CG model has been tested on several systems, including the HIV-1 protease flap opening and ligand binding (22,28–30) and the ribosome dynamics (31). It has been compared against all-atom (26) and implicit solvent (29) MD simulations and yielded results that are in good agreement with both.

In our CG simulations, the degree of complexity and some unique features presented by the AChEt necessitated a number of modifications to be made. For example, as the model lacks the screening effect of explicit water molecules, the electrostatic interactions between two charged amino acids on the protein surface, Asp^{310} of the catalytic domain and Arg^{551} of the WAT, occasionally become too strong. We thus introduced a weak Morse potential for this pair to avoid unrealistically close distances between them (see Supplemental Material for parameters). A cutoff of 15 Å was set for both nonbonded terms. Furthermore, the WAT helices possess a special WWW motif making strong hydrophobic stacking with the PRAD. There are also disulfide bonds within a monomer and between monomers and ColQ. To capture these special interactions which are much stronger than typical vdW interactions, a harmonic form, $k_r(r - r_0)^2$, is applied to replace the Morse potential in Eq. 1, where r is the distance between two interaction beads. Probability distribution functions for r were obtained from the 20 ns AA-MD simulation, which provided force constants, k_r, of, e.g., ~41 kcal/mol Å^2 for a Pro-Trp stacking pair (Supplementary Material).

Brownian dynamics

Three snapshots from the AA-MD simulation collected at 1.16, 7.72, and 14.72 ns were used to initiate BD simulation runs I, II, and III, respectively. The use of several snapshots ensures that, first, the model-built (AChEt) structure has become sufficiently relaxed that any remaining bad contacts are removed. Second, as some of the parameters for the CG-BD runs are derived from the initial structure, alternative starting conformations reduce undue dependence on the initial conditions. Furthermore, different random number seeds were assigned to an initial conformation to increase sampling. The BD simulations were run for 10 μs or 15 μs. The time step was set to 0.1 ps, and the viscosity of water was set to 1 cp, which corresponds to a water temperature of 293 K. The BD algorithm used here has been reported in several original publications (32,33), and all the parameters and equations can be found in a previous publication (29).

Analysis

Intrasubunit structural properties

Deviation from the initial model and the structural integrity of each individual subunit during the simulations was monitored by the root mean-square deviations (RMSD). The fluctuations within a subunit were studied using the root mean-square fluctuations (RMSF).

Block normal mode and principal component calculations

The method used to compute BNM, where each residue is treated as a block, has been published previously (34). The method has also been applied on the AChEt model (12). The BNMs were calculated for four selected snapshots from the AA-MD simulation. We chose the last snapshot and the three snapshots used for starting independent CG-BD runs. PCA was carried out for the CG-BD trajectories using the structural analysis program Bio3D and its default parameters (35).

Large-scale intersubunit fluctuations

To investigate the large-scale intersubunit dynamics, three variables were defined (Fig. 1): the distance (d) between the center of mass of subunits in contact with one another (cf. A-B, B-C, C-D, and D-A); the angle (θ) subtended by vectors connecting the center of a subunit to the centers of the other two subunits it is in contact with (cf. $D\hat{A}B, A\hat{B}C, B\hat{C}D$, and $C\hat{D}A$); and interfacial contact (χ), defined as the average of the number of atoms in subunit i within 10 Å of any atom in complementary subunit j, and the number of atoms in j that are within 10 Å of any atom in i. As illustrated in Fig. 1 (*right*), χ is the intersection between two selections and represents contacts of surface atoms only. We obtained the same results by using the interfacial surface area of a subunit occluded from solvent by an opposing subunit (see Supplementary Material). To calculate the change in solvent-accessible surface area (ΔSASA) from the CG-BD trajectories, the CG bead radii (which account for the size of each residue) were introduced into the CHARMM parameter file. Then, the solvent-accessible surface for individual subunits and for pairs of subunits (dimer) was computed with the CHARMM program (36), using the new radii and a regular probe radius of 1.4 Å. ΔSASA of subunit A due to subunit B is then obtained by subtracting the SASA of the dimer A-B from the sum of SASAs of subunits A and B in isolation.

Active site occlusion

As a qualitative measure of occlusion of the active site of a subunit by a complementary subunit, we checked for the number of atoms in subunit j that are within 16 Å (approximately twice the average length of a residue plus the radius of ACh) of the peripheral anionic site (PAS) residues Tyr^{72}, Trp^{286}, and Tyr^{341} residing in subunit i. These residues were selected because they can interact with a flexible loop in a complementary subunit in the tetramer (5). We would like to stress that although the three residues Tyr^{72}, Trp^{286}, and Tyr^{341} at the PAS are preselected, the occlusion as defined here is a dynamic measure that for each frame counts all atoms in an opposing subunit that make contact (cutoff 16 Å) with the preselected fixed residues. This can occur through translation and/or rotation of subunits or through local movements of surface loops or through a combination of all three.

Gating effects

The intersubunit motions may serve as a gate to control binding site accessibility. In this study, we assume that the active sites have two states, open and closed, which may be described as follows:

$$open \underset{k_o}{\overset{k_c}{\rightleftarrows}} closed, \qquad (2)$$

where k_o and k_c are gate opening and closing rate constants, respectively. According to the rate theory for gated binding of ligands to proteins (37,38), the gated association rate constants may be written as

$$k_G = k_{UG}\frac{k_o}{k_c + k_o}, (k_c + k_o)^{-1} \gg \tau_d \quad (3)$$

$$k_G = k_{UG}, (k_c + k_o)^{-1} \ll \tau_d \quad (4)$$

$$\tau_d = \frac{r_c^2}{D}, \quad (5)$$

where r_c is the collision distance between the two molecules, D is their relative translational diffusion constant, and τ_d is the characteristic diffusional relaxation time of the molecular system. ''Slow gating'' occurs if the opening and closing of the gate is much slower than τ_d. The gated association rate constant k_G is then approximated by multiplying the opening fraction by the ungated association rate constant k_{UG} (see Eq. 3). ''Fast gating'' occurs if the gate fluctuation is faster than the characteristic time for diffusion. In a fast gated system, it appears to the ligand that the binding site is always open, thus k_G is equal to k_{UG} (Eq. 4).

RESULTS

We first present the intrasubunit structural properties during the simulations. Then, we present the large-scale motions as suggested by normal mode analysis and PCA, followed by the analysis of the intersubunit rotational and translational motions together with interfacial properties. We will then show how the intersubunit fluctuations affect access to active centers. As we are interested mainly in the large-scale intersubunit motions that would affect the accessibility of the active sites to substrates, in the following we focus on the four catalytic domains (residues 1–543) only, unless specifically mentioned. Note that many CG-BD simulations were carried out, but only one representative run (run II) is shown in Figs. 2–4 and 6.

Intrasubunit structural properties

Examples of the RMSD and RMSF derived from AA and CG simulations are plotted in Fig. 2 for each individual subunit. We can see that the subunits are stable in both the AA and CG simulations (Fig. 2 *A*). The RMSD rose to 4 Å in the 20 ns production run of the AA simulation, whereas the CG simulation fluctuated between 2 and 5.5 Å. Although the values appear somewhat high, they are reasonable for a system of this size. Furthermore, some reorganization is expected upon the relaxation of the initial model. As expected, however, the AA-MD run is not yet fully equilibrated, although it is sufficiently stabilized for the purposes of this work. Note that the CG simulations, including the one displayed in Fig. 2, were started from a snapshot of the AA simulation; thus the starting conformation had already moved away from the initial model.

The calculated RMSFs show that both simulations suggest substantial internal mobility of the subunits (Fig. 2 *B*). For example, consistent with previous studies (5,39,40), the Ω-loop (residues 257–272) (39) exhibits significant mobility in all cases. Although the RMSF of the Cα atoms derived from the AA simulations is higher for a number of residues, the similar pattern between the AA and CG simulations suggests that the extremely fast CG model qualitatively captures the most relevant motions suggested by the AA-MD. The CG model was expected primarily to sample the long timescale low frequency motions; differences in, for example, time steps (2 fs vs. 100 fs) between AA-MD and CG-BD imply that fluctuations would not be identical.

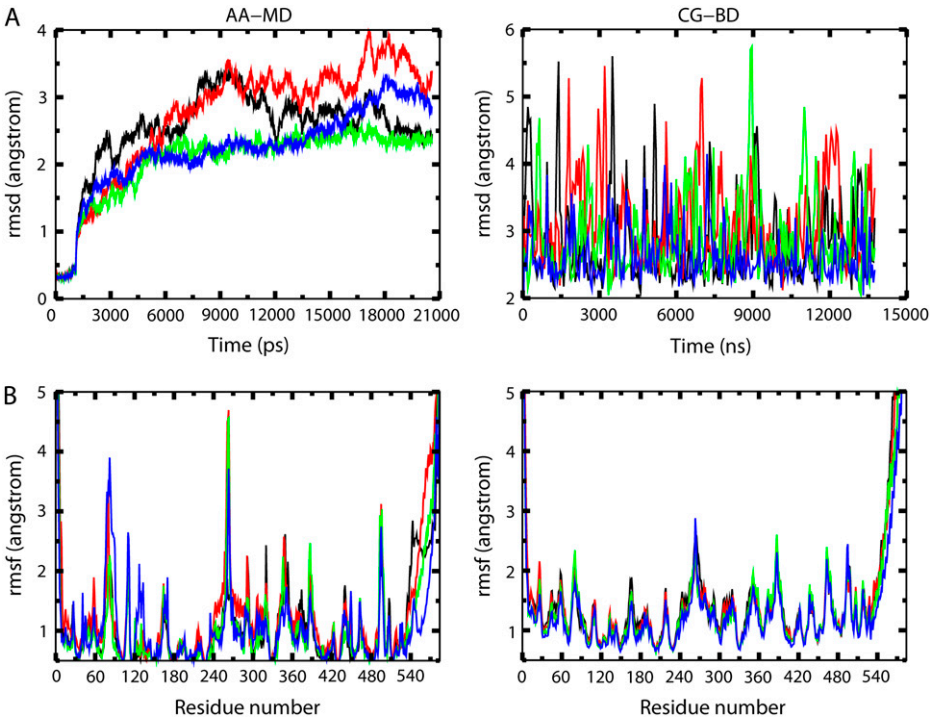

FIGURE 2 Time evolution of AChEt catalytic subunits' (residues 5–543, excluding the WAT domain) structural properties during the 20 ns AA-MD (*left*) and one of the (CG-BD, *right*) simulations. (*A*) RMSD and (*B*) RMSF in Å calculated after individually fitting the Cα atoms of each catalytic subunit. Color code: A (*black*), B (*red*), C (*green*), and D (*blue*).

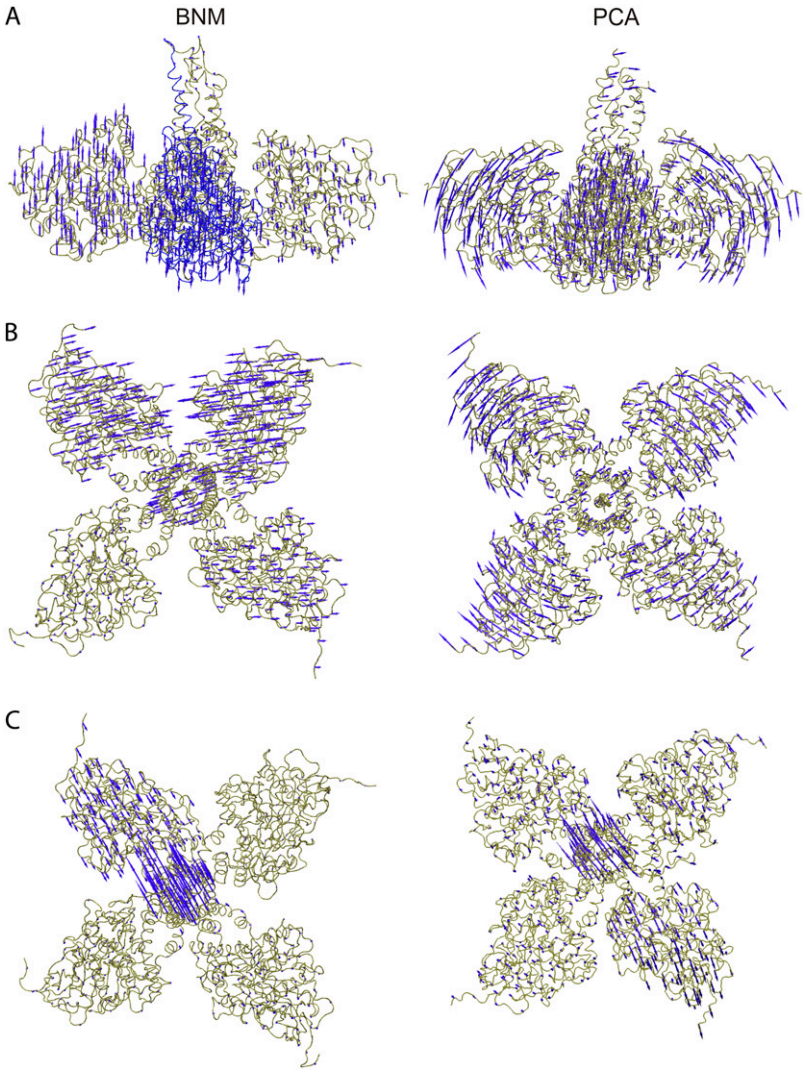

FIGURE 3 BNM (*left*) and PCA (*right*). The BNMs were calculated for all three snapshots used for starting the CG-BD runs as well as for the last snapshot; a representative result from a snapshot at 7.72 ns, which was used to start run II, is shown here. Similarly, the PCA shown here is only for run II. The rest of the BNM and PCA calculations are very similar. (*A–C*) Representative modes from the first, second, and third sets of lowest frequency BNMs (see text) and the first, second, and third PCs. The blue arrows, drawn every four residue for clarity, indicate the direction of motion. For each mode (i.e., for those in *A*, *B*, and *C*), the same orientation is used and for different modes (i.e., *A* versus *B*, etc.), structures are rotated for the best view.

Low-frequency motions from normal mode and principal component analyses

The initial structure used in this study was a model built from two x-ray structures of different resolutions (1C2O and 1VZJ). BNM analysis performed on the model suggested large-scale motions. To investigate whether those motions are preserved when the structure evolves during the MD simulation, we recomputed the BNM on four selected AA-MD snapshots. We found nine low-frequency normal modes (excluding translation and rotation) that can be grouped into three sets (or types of motions), each of which contain three modes (see Supplementary Fig. S2). On the whole, the first and second sets represent out-of-plane and in-plane motion of the catalytic domains, respectively, whereas the third set accounts for a ''swinging'' motion of the WAT domain (Fig. 3). The three modes within a set represent essentially the same motion in orthogonal directions with barely separated eigenvalues. We found the same type of motions in all four snapshots except for switches in the order of modes within the same set. This is to be expected because modes within a set are almost degenerate, with the three types of large-scale motions remaining as the most relevant fluctuations. These motions are similar to those reported earlier that were based on BNM analysis of the model-built structure (12). Most interestingly, the first three principal components computed from the CG-BD trajectories closely match the results from the BNM analysis (Fig. 3). These results clearly show that there are few low-frequency motions involving translation, rotation, and bending deformations that account for the major conformational changes in AChEt. Furthermore, similarity of the BNM results among different AA-MD snapshots and between the AA-MD relaxed structures and the initial model indicates that the motions are robust with regard to fine structural details and thus unaffected by deficiencies potentially present in the initial model of the AChEt. This is further reinforced by the similarity between the BNM and the

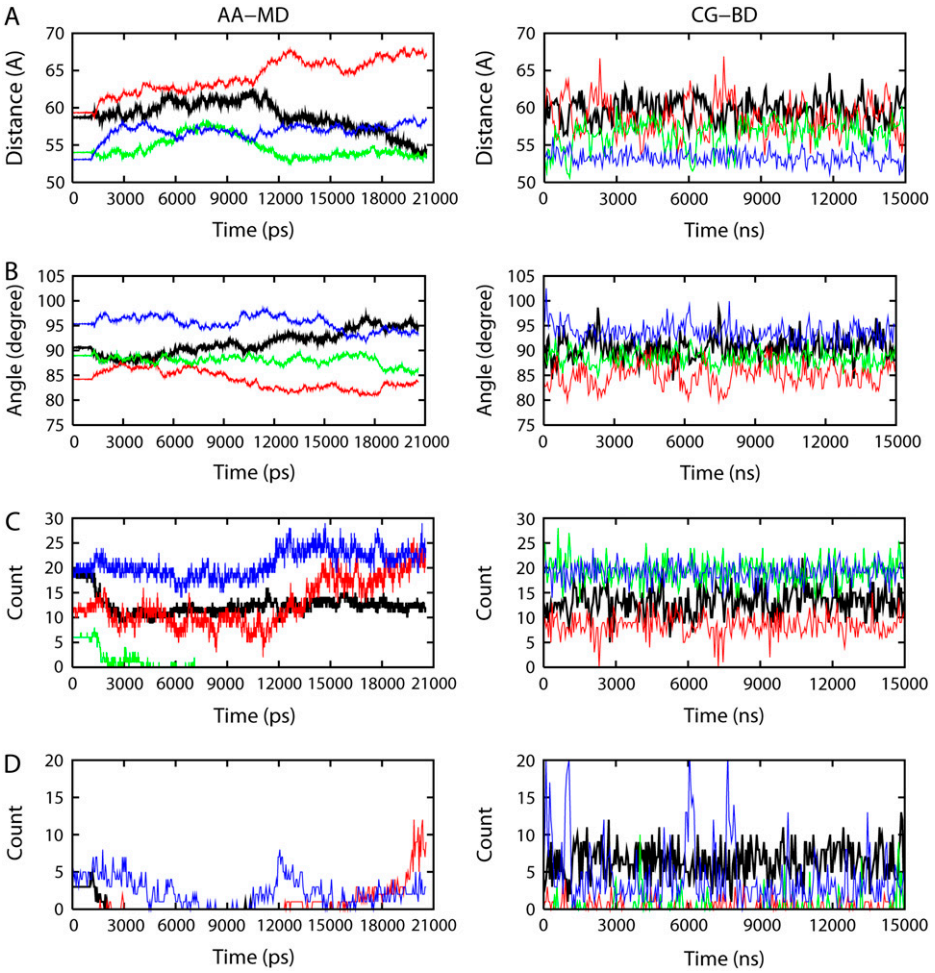

FIGURE 4 Distance (d), angle (θ), number of interfacial contacts (χ), and occlusion involving the catalytic domains (residues 5–543). (*A*) d between the center-of-mass of two subunits: A-B (*black*), B-C (*red*), C-D (*green*), and D-A (*blue*). (*B*) θ subtended by the centers of three subunits: $D\hat{A}B$ (*black*), $A\hat{B}C$ (*red*), $B\hat{C}D$ (*green*), and $C\hat{D}A$ (*blue*). (*C*) χ defined as the mean of the numbers of atoms in subunit i within 10 Å of any atom of subunit j and vice versa: A-B (*black*), B-C (*red*), C-D (*green*), and D-A (*blue*). (*D*) Occlusion defined as the number of atoms in a complementary subunit j within 16 Å of the PAS residues 72, 286, and 341 of subunit i: A (*black*), B (*red*), C (*green*), and D (*blue*).

PCA results, which also validate the capability of our CG model to capture the relevant large-scale motions.

Measuring the large-scale intersubunit motions

The time evolutions of the intersubunit distance (d), angle (θ), and interfacial contact (χ) in the course of the AA and CG simulations are shown in Fig. 4, *A–C*. The plots show that first, the subunit arrangement is asymmetric and there is indeed a substantial intersubunit movement. Second, both the AA and CG simulations sample a similar range of distances (Fig. 4 *A*) and angles (Fig. 4 *B*). Third, compared with what was accessible by the short AA-MD run, the fast and highly simplified CG runs sampled various arrangements of subunits, achieving equilibrium fluctuations in which a conformational space is reversibly revisited. For example, d between subunits A and B (A-B) was >65 Å in the first 10 ns of AA-MD but subsequently dropped to <55 Å, whereas subunits B and C kept moving apart. In contrast, the CG-BD run sampled the whole range of distances, roughly between 52 and 65 Å for both A-B and B-C. An even larger conformational space was sampled by running several CG-BD simulations. Similar information is obtained using the variable θ, where the asymmetry and dynamics of the subunit arrangement is clearly seen in Fig. 4 *B*. The subunits rotate substantially relative to one another, such that a significant proportion of the conformations adopt a nonplanar subunit arrangement. As mentioned before, both (pseudosquare) planar and nonplanar subunit arrangements have been observed by x-ray crystallography (6). It is therefore instructive to quantify the extent of nonplanarity in the simulated structures. To characterize deviation from planarity, the difference between the sum of all four angles in AChEt and 360° has been calculated. Fig. 5 displays histograms of the deviation from planarity. For comparison, the nonplanarity calculated for the nonplanar crystallographic structure (1C2O) is 3°, which is shown in the figure as a magenta dashed line. We find that 27%, 15%, and 26% of all the collected snapshots from the CG-BD runs I, II, and II, respectively, are even more nonplanar than 1C2O. Using a more relaxed cutoff of 1°, over 50% (i.e., 70%, 51%, and 60%) of the structures are nonplanar. These data clearly show that AChEt fluctuates between planar and nonplanar subunit arrangements and that x-ray structures 1C2O and

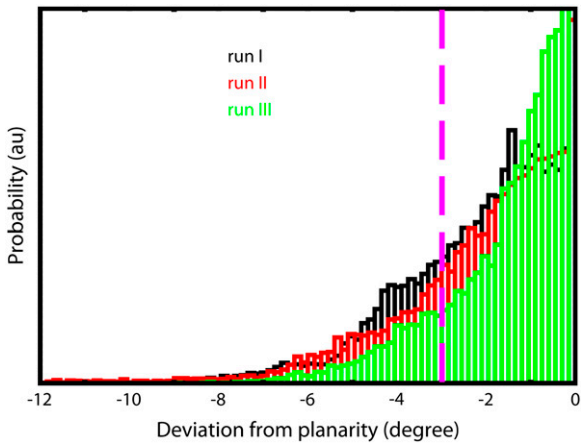

FIGURE 5 Histograms of the deviations from planarity, defined as $\sum_{k=1}^{4}\theta_k - 360$, where θ is as defined in the legend of Fig. 4 and k is an index for the angles. The magenta dashed line represents the nonplanarity of the x-ray structure 1C2O.

12CB represent individual snapshots of the available conformations in solution.

In addition to studying the fluctuations of the catalytic domains in terms of a rigid-body motion, it is important to investigate how the local contacts at the subunit interfaces (χ) behave. There are a variety of ways to quantify the interfacial contacts. We used the variable χ as defined in Methods. Furthermore, since the value of χ and its ability to exclude buried atoms depends on the arbitrary cutoff used, we checked the change in SASA upon the association of two subunits. Essentially the same results were obtained (see Supplementary Fig. S2). Therefore, with the current cutoff (10 Å), χ is a good measure of interfacial contact; its time evolution is shown in Fig. 4 *C*. The plot shows substantial fluctuation in both the AA and CG simulations. Occasionally, the contact between subunits B and C is lost. In fact, several CG runs indicate that any two pairs of subunits tend to have tighter interaction (higher χ) than the remaining two pairs. Furthermore, as in the case of the distances and the angles, the number of contacts between subunits varies from pair to pair. For example, all three variables (d, θ, χ) display higher fluctuation when subunit B is involved in the measurement. Taken together, these data demonstrate that AChEt is significantly dynamic due to the weak interaction between the catalytic subunits that allows translational and rotational motions of the subunits relative to one another.

Peripheral anionic site occlusion

The major goal of this work is to elucidate the nature and extent of active site occlusion by neighboring subunits. To monitor active site occlusion due to a complementary subunit, it is important to identify which of the gorge residues are affected upon tetramer formation. Buried residues, such as those lining the gorge, are inaccessible to residues in an opposing subunit. Although these residues experience high-frequency internal fluctuations that may play a role in accommodating a bound substrate, such fluctuations would not affect occlusion as defined here. Among the surface residues that play a critical role in substrate capture and binding, Tyr^{72}, Trp^{286}, and Tyr^{341} at the PAS were found to consistently become blocked by residues from an opposing subunit (41). Therefore, contacts to these three residues by any residue of an opposing subunit can be a good estimate of the degree of occlusion. We therefore defined occlusion as the number of atoms in an opposing subunit that are within 16 Å of the three PAS residues of a particular subunit (see Methods). The results are shown in Fig. 4 *D*. In these plots, the higher the number, the more occluded the active site would be. We can see that the peripheral sites of subunits A and D become frequently occluded by subunits D and C, respectively (Fig. 4 *D*). Further, although the fractions of occluded PAS vary among the subunits, the active sites of subunits B and C are accessible more frequently than those of subunits A and D. Similar results were obtained in all three CG-BD runs.

Overall, the presented data clearly show that the intersubunit fluctuations are intrinsic properties of the tetramer. Such a dynamic assembly of the subunits permits individual subunits to experience events of occlusion and opening the extent and rate of which varies among the subunits. These issues will be discussed further in the following sections.

DISCUSSION

Multiscale simulations to explore large-scale spatiotemporal fluctuations

The large-scale intersubunit motions cannot be fully captured by nanoseconds-long AA-MD simulations; the size of the system (~2400 residues) prohibits sufficient sampling. We therefore decided to approach the problem by combining AA-MD and Cα-based CG-BD simulations. There are two advantages to this approach: we can i), improve the parameterization of the CG model using data from the AA simulation, and ii), exploit the extensive sampling power of the CG model for investigating the long timescale dynamics of AChEt. To be able to handle the very large and complicated structure of the AChEt, we made a number of modifications on the CG model with the help of results from the AA-MD (see Methods). First, the AA-MD provided the parameters for the harmonic constraints between the unusually tightly bound PRAD-WAT helices. This modification helped to create a stable structure of the PRAD-WAT region without affecting the structure and dynamics of the globular catalytic subunits. Second, due to the lack of electrostatic screening by the high dielectric water, Arg^{551} of the WAT domain becomes locked in interaction with a surface residue Asp^{310} in the catalytic domain. This was prevented by applying a Morse potential between the two residues based on their

average separation in the AA simulation. The computational efficiency of the CG model allowed several CG-BD runs to be performed using several AA-MD-relaxed structures as starting conformations, thus reducing dependency on initial conditions.

After the required parameterizations, the CG-BD simulations both captured the large-scale motions (Figs. 3–5) and, as illustrated in Fig. 4 *D*, allowed an extensive sampling of conformational space that was inaccessible to the AA-MD; important regions were visited repeatedly. For example, the AA simulation achieved only one and two events of PAS occlusion at subunits B and D, respectively, but none at subunits A and C. In the BD simulations, many events of occlusion and opening, most prominently in subunit D, have been achieved. The latter enables analysis of some of the equilibrium and kinetic properties of the tetramer (discussed below). Therefore, the multiscale simulations provided information that went beyond the capabilities of either the AA or CG model alone. Yet, despite their profoundly different spatial and temporal scales, the two models complement one another, as evidenced by the above examples.

Furthermore, we calculated the normal modes for selected snapshots from the AA-MD simulation. We found nine low-frequency modes (Fig. 3) which represent different flavors of three major motions. The first three represent rotation-dominated ''shearing'' of the catalytic domains relative to one another. The second set of modes represents a largely translational in-plane motion of the catalytic domains. The third set accounts for the ''swinging'' motion of the WAT helices. To investigate whether the major movements are altered during the simulation, we compared the BNM obtained from several snapshots. We found that except for small exchanges in the eigenvalues within a given set, there are no significant changes in the type of motion. To further check this issue, we computed the principal components from the CG-BD simulations (Fig. 3). As expected, the low-resolution CG model was not able to resolve the small differences observed within a given set. Remarkably, however, the three major motions seen in the BNM are faithfully reproduced. Therefore, the large-scale motions involving subunits of the tetramer, which were implied by AA-MD and captured by both the BNM and CG-BD simulations, are intrinsic properties of the enzyme.

Local versus global effects

Having discussed the reliability of the CG model and the initial structure, as well as the conformational sampling afforded by the multiscale simulations, we would like to investigate the structures to determine which of the motions, localized high-frequency interfacial fluctuations or large-scale domain motions, are more important for the function of the tetrameric enzyme. Inhibitors that bind to the PAS at the entrance to the active site gorge (42) influence catalysis by blocking entrance of ligands and removal of products (1,5,43–47). In the tetramer, a similar blockade could come from a nearby subunit. For example, in the mouse tetramer, which is compact and pseudosquare planar (5), the Gly^{260}–Gly^{264} cluster of hydrophobic residues at the tip of the short Ω-loop (39) pack against the PAS residues Tyr^{72}, Trp^{286}, and Tyr^{341}, sterically occluding access to the active center gorge. Similarly, in the compact eAChE tetramer (1C2O), two of the gorges from diagonally opposed subunits face the tetramer internal space, with their PAS occluded. In contrast, the loose eAChE tetramer (1C2B), despite its resemblance to the mAChE tetramer in terms of the pseudosquare planar arrangement of the subunits, has all four active centers fully accessible to solvent. Therefore, occlusion of the PAS is dependent on the translations and rotations of the subunits relative to one another but can also be modulated by local conformations such as those of the Ω-loop or other surface loops. Therefore, to determine whether or not the global intersubunit fluctuations are more important for the occlusion of the PAS than the local interfacial motions, we plotted the occlusion against the intersubunit distance (Fig. 6, *main plot*) and the interfacial contacts (Fig. 6, *inset*). There is a reasonably strong anticorrelation between occlusion and distance (correlation coefficient, $R = -0.78$) but none between occlusion and interfacial contact. There was no correlation with the interfacial surface area either (ΔSASA, see Supplementary Fig. S3). Therefore, the simulations suggest that occlusion is a function of intersubunit fluctuations and that the rate of blockade and opening of the route to the active center is regulated mostly by the motions of the subunits relative to one another.

Functional implications of the dynamics

The tetramer is the major functional form of AChE in cholinergic synapses, though tetramerization may affect ligand

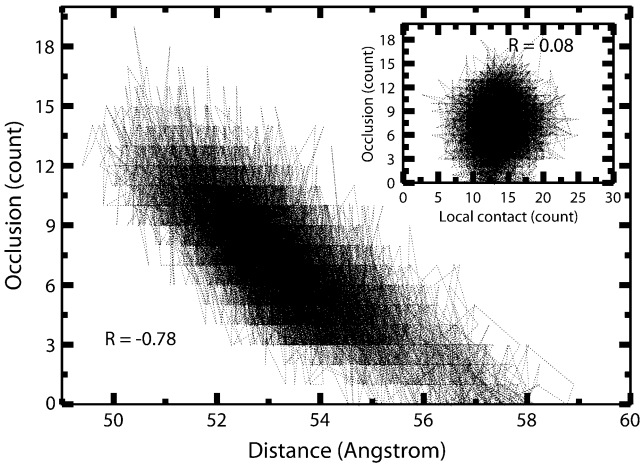

FIGURE 6 Plots of occlusion against the intersubunit distance (main plot) and interfacial contact (*inset*) for the A-D pair. The correlation coefficients are indicated. A similar behavior was obtained for the other subunit pairs.

accessibility to the peripheral site (2,48,49). Our simulations show that the subunits are highly dynamic and that alternative opening and occlusion of an active site is allowable. This would imply that instead of being trapped in an occluded active site, for which ligand binding is limited, the subunits fluctuate relative to each other to expose all four active sites.

The accessibility of an active site may be divided into three states based on the probability distribution of the active site occlusion (Fig. 7 *A*). The first of these, the open state, has an occlusion number <2. The second, which has an occlusion number between 2 and 5, is considered partially open. The third one, the occluded state, covers an occlusion number >5. For example, in the crystal structure 1C2O, two of the four active sites are in the open and two are in the occluded state (occlusion numbers are both 9) whereas in 1C2B, all four active sites are open (occlusion numbers are 0). This definition is reasonable, as demonstrated by ACh-protein docking. Fig. 8 illustrates the docking results using the Vdock package (50,51). ACh was always docked near the entrance to the active site when AChE was in the open state. In the partially open state, ACh was placed mostly near the entrance, but the molecule could also be trapped by the complementary subunit. ACh can still reach the PAS when an active site is occluded, but it is very likely to interact and stay with the complementary subunit (Fig. 8). As a result, the association may be reduced by occlusion. Although it may be more efficient for catalysis to keep the four active sites always in the open state, the (weak) intersubunit interactions and thermal fluctuations bring two subunits close enough to hinder ligand binding, as shown in Fig. 8.

Fig. 7 *B* shows partially open (i.e., partially occluded) and fully open fractions computed from four BD runs. The fractions of fully open conformations vary between subunits, and the average value is ~52%. This suggests that, on average, two open states may be observed in the tetramer. However, in contrast to the crystal structures where only subunits B and D are in the open state, our BD simulations reveal that all four active sites can adopt three different conformational states, albeit with varying populations. Such dynamics may provide more symmetric binding sites for the tetramer, as compared with the axially asymmetric binding sites in 1C2O. It is worth noting that most conformations generated by the simulations are not very close to structures 1C2O or 1C2B. Zhang et al. generated an intermediate structure INT by morphing between the two crystal structures. Their calculation suggested that reaction rates for INT and 1C2B are similar, whereas the more compact 1C2O has slower rates (7,8). As a result, although all four active sites may not be in their open state simultaneously, the conformational dynamics may enable the tetramer to retain rates similar to those of 1C2B.

Finally, it is of interest to investigate if the binding of ACh is ''gated'' by intersubunit motions. Eq. 2 is applied here; thus we classify the partially and fully open states as an open gate, whereas we consider the occluded state a closed gate. The calculated average dwell times of the open gate and closed gate are ~300 ns and ~50 ns, respectively. The opening and closing rate constants k_o and k_c of this system are thus 1/50 and 1/300 ns^{-1}. The computed $(k_o + k_c)^{-1}$ is a few orders of magnitude larger than the diffusional relaxation time (see Eq. 5) if we assume that the protein and ACh have approximate radii of 65 Å and 3 Å, respectively. Thus, according to Eq. 3, the intersubunit motions may be viewed as ''slow gating'', and the gated association rate constant may therefore be estimated by the ungated rate constant multiplied by the opening fraction. The approximate gated rate constant here is ~85% of that for an ungated active site. We may also view the number as though one of the four active sites is closed, on average, during the approach of ACh to the tetramer. This result is consistent with the experimental finding that the binding of a substrate to the PAS is only somewhat hindered by the association of the subunits (49), resulting in a slightly higher substrate inhibition constant (48) in the tetramer than in the monomer (49). Note that our method provides reasonable approximations in subunit motions. However, since the CG models do not have explicit water molecules, the timescales exhibited here might not correspond exactly to those in cells. It is also important to underline that the arrangement of the subunits in the tetramer is asymmetric, as illustrated by a comparison between the initial nearly symmetric model (Fig. 1 *A*) and the MD relaxed structure (Fig. 8 *A*). Note also that the effect of electrostatics, which was shown to enhance the rate of binding (7), is not

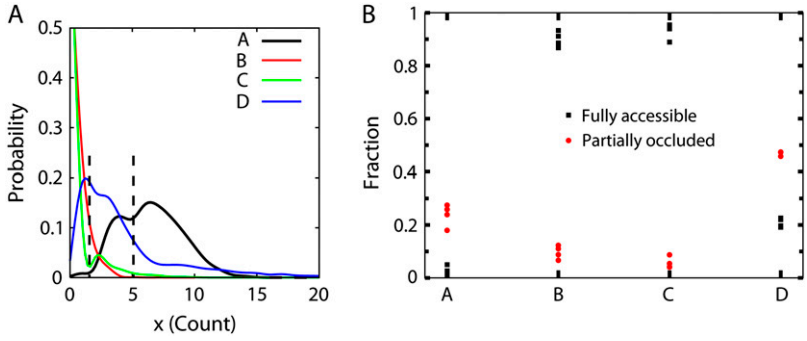

FIGURE 7 Statistical analysis of the PAS occlusion. (*A*) Probability distribution of the occlusion in one of the CG-simulations. Vertical dashed lines indicate the cutoffs used to define three states represented by the snapshots having an occlusion less than or equal to 2 (state 1), between 2 and 5 (state 2), or greater than 5 (state 3). (*B*) The fraction of structures in state 1 (*square*) and state 2 (*circle*) for subunits A, B, C, and D derived from each of the four CG-BD runs.

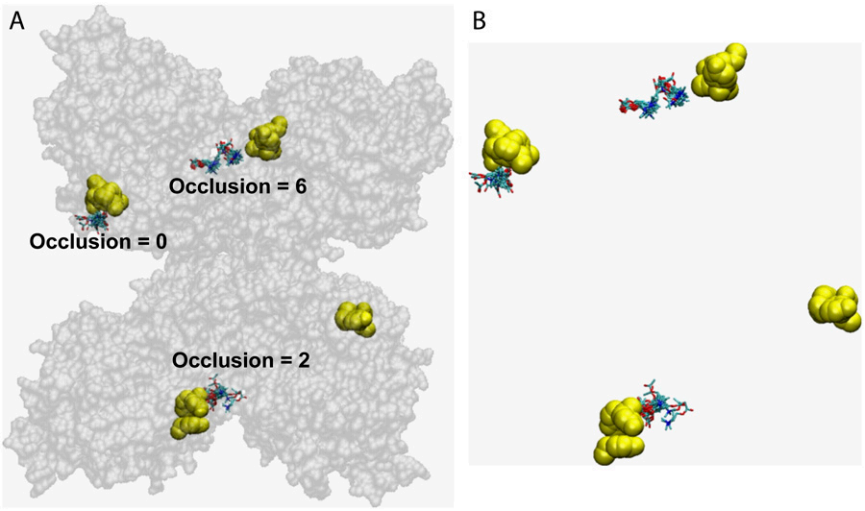

FIGURE 8 Docking of ACh into the PAS of AChE. (*A*) Docking results. Two hundred ACh structures were docked into three of the four PASs representing the open (occlusion = 0), partially occluded (occlusion = 2), and occluded (occlusion = 6) states. See text and legends of Figs. 1 and 5 for the definitions of PAS and occlusion. (*B*) A zoom-in on the PAS residues and the ACh structures docked onto PAS.

considered here. Only the geometry of the tetramer is discussed as having a gating effect. Taken together, the catalytic activity of each subunit might not be very adversely affected by the tetramer formation, as has also been suggested by experiments (49). Moreover, the tetramer provides more active sites that, for an approaching ACh, present at least three times greater a chance for reaction than an isolated monomer.

CONCLUSION

In this work, we presented results from multiscale simulations that allowed us to directly connect long timescale domain motions with the active site substrate accessibility of the enzyme AChE. The in-plane translation and out-of-plane rotational motions of the four catalytic domains lead to dynamic occlusions of the peripheral cationic site. These motions gate substrate-protein association and allow the active center to be accessible for more than 80% of the time on average. A combination of methods involving atomistic and CG simulations as well as normal mode analyses was used to establish the link between domain motion and substrate accessibility. This approach is likely to be useful for future investigations of biomolecular systems. The results also lay the foundation for further study on the role of tetramerization in the catalytic efficiency of AChE, which may include rate calculations on several structures representing different active site occlusions.

SUPPLEMENTARY MATERIAL

To view all of the supplemental files associated with this article, visit www.biophysj.org.

We thank Drs. T. Shen, Y. Cheng, D. Zhang, B. Lu, V. Tozzini, and J. Trylska for discussions and suggestions, the San Diego Supercomputer Center for computational resources, and Verachem for the use of the Vdock package.

A.A.G. acknowledges financial support from the Commission for the Promotion of Young Academics of the University of Zurich. Additional support was provided by the National Science Foundation, National Institutes of Health, Howard Hughes Medical Institute, National Biomedical Computation Resource, Center for Theoretical Biological Physics, and Accelrys.

REFERENCES

1. Sussman, J. L., M. Harel, F. Frolow, C. Oefner, A. Goldman, L. Toker, and I. Silman. 1991. Atomic structure of acetylcholinesterase from Torpedo californica: a prototypic acetylcholine-binding protein. *Science*. 253:872–879.
2. Johnson, G., and S. W. Moore. 2006. The peripheral anionic site of acetylcholinesterase: structure, functions and potential role in rational drug design. *Curr. Pharm. Des.* 23:217–225.
3. Rieger, F., S. Bon, and J. Massoulie. 1973. Electron microscopic studies on stretched and globular acetylcholinesterase molecules of the electric eel (Electrophorus electricus). *Eur. J. Biochem.* 34:539–547.
4. Cartaud, J., F. Rieger, S. Bon, and J. Massoulie. 1975. Fine structure of electric eel acetylcholinesterase. *Brain Res.* 88:127–130.
5. Bourne, Y., P. Taylor, P. E. Bougis, and P. Marchot. 1999. Crystal structure of mouse acetylcholinesterase. A peripheral site-occluding loop in a tetrameric assembly. *J. Biol. Chem.* 274:2963–2970.
6. Bourne, Y., J. Grassi, P. E. Bougis, and P. Marchot. 1999. Conformational flexibility of the acetylcholinesterase tetramer suggested by x-ray crystallography. *J. Biol. Chem.* 274:30370–30376.
7. Zhang, D., J. Suen, Y. Zhang, Y. Song, Z. Radic, P. Taylor, M. J. Holst, C. Bajaj, N. A. Baker, and J. A. McCammon. 2005. Tetrameric mouse acetylcholinesterase: continuum diffusion rate calculations by solving the steady-state Smoluchowski equation using finite element methods. *Biophys. J.* 88:1659–1665.
8. Cheng, Y., J. K. Suen, D. Zhang, S. D. Bond, Y. Zhang, Y. Song, N. A. Baker, C. L. Bajaj, M. J. Holst, and J. A. McCammon. 2007. Finite element analysis of the time-dependent Smoluchowski equation for acetylcholinesterase reaction rate calculations. *Biophys. J.* 92:3397–3406.
9. Massoulie, J., S. Bon, N. Perrier, and C. Falasca. 2005. The C-terminal peptides of acetylcholinesterase: cellular trafficking, oligomerization and functional anchoring. *Chem. Biol. Interact.* 157–158:3–14.
10. Falasca, C., N. Perrier, J. Massoulie, and S. Bon. 2005. Determinants of the t peptide involved in folding, degradation, and secretion of acetylcholinesterase. *J. Biol. Chem.* 280:878–886.

11. Dvir, H., M. Harel, S. Bon, W. Q. Liu, M. Vidal, C. Garbay, J. L. Sussman, J. Massoulie, and I. Silman. 2004. The synaptic acetylcholinesterase tetramer assembles around a polyproline II helix. *EMBO J.* 23:4394–4405.
12. Zhang, D., and J. A. McCammon. 2005. The association of tetrameric acetylcholinesterase with ColQ tail: a block normal mode analysis. *PLoS Comput. Biol.* 1:e62.
13. Hasinoff, B. B. 1982. Kinetics of acetylthiocholine binding to electric eel acetylcholinesterase in glycerol/water solvents of increased viscosity. Evidence for a diffusion-controlled reaction. *Biochim. Biophys. Acta.* 704:52–58.
14. Silman, I., M. Harel, P. Axelsen, M. Raves, and J. L. Sussman. 1994. Three-dimensional structures of acetylcholinesterase and of its complexes with anticholinesterase agents. *Biochem. Soc. Trans.* 22:745–749.
15. Kremer, K., and F. Muller-Plathe. 2002. Multiscale simulation in polymer science. *Mol. Simul.* 28:729–750.
16. Muller-Plathe, F. 2002. Coarse-graining in polymer simulation: from the atomistic to the mesoscopic scale and back. *ChemPhysChem.* 3: 754–769.
17. Yang, S., H. Levine, J. N. Onuchic, and D. L. Cox. 2005. Structure of infectious prions: stabilization by domain swapping. *FASEB J.* 19: 1778–1782.
18. Levy, Y., and J. N. Onuchic. 2006. Mechanisms of protein assembly: lessons from minimalist models. *Acc. Chem. Res.* 39:135–142.
19. Chu, J. W., S. Izveko, and G. A. Voth. 2006. The multiscale challenge for biomolecular systems: coarse-grained modeling. *Mol. Simul.* 32:211–218.
20. Ayton, G. S., and G. A. Voth. 2007. Multiscale simulation of transmembrane proteins. *J. Struct. Biol.* 157:570–578.
21. Tozzini, V. 2005. Coarse-grained models for proteins. *Curr. Opin. Struct. Biol.* 15:144–150.
22. Tozzini, V., J. Trylska, C. E. Chang, and J. A. McCammon. 2007. Flap opening dynamics in HIV-1 protease explored with a coarse-grained model. *J. Struct. Biol.* 157:606–615.
23. Gorfe, A. A., and A. Caflisch. 2005. Functional plasticity in the substrate binding site of beta-secretase. *Structure.* 13:1487–1498.
24. Phillips, J. C., R. Braun, W. Wang, J. Gumbart, E. Tajkhorshid, E. Villa, C. Chipot, R. D. Skeel, L. Kale, and K. Schulten. 2005. Scalable molecular dynamics with NAMD. *J. Comput. Chem.* 26:1781–1802.
25. MacKerell, A. D., D. Bashford, M. Bellott, R. L. Dunbrack, J. D. Evanseck, M. J. Field, S. Fischer, J. Gao, H. Guo, S. Ha, D. Joseph-McCarthy, L. Kuchnir, K. Kuczera, F. T. K. Lau, C. Mattos, S. Michnick, T. Ngo, D. T. Nguyen, B. Prodhom, W. E. Reiher, B. Roux, M. Schlenkrich, J. C. Smith, R. Stote, J. Straub, M. Watanabe, J. Wiorkiewicz-Kuczera, D. Yin, and M. Karplus. 1998. All-atom empirical potential for molecular modeling and dynamics studies of proteins. *J. Phys. Chem. B.* 102:3586–3616.
26. Tozzini, V., and J. A. McCammon. 2005. A coarse grained model for the dynamics of flap opening in HIV-1 protease. *Chem. Phys. Lett.* 413: 123–128.
27. Davis, M. E., J. D. Madura, B. A. Luty, and J. A. McCammon. 1991. Electrostatics and diffusion of molecules in solution—simulations with the University-of-Houston-Brownian dynamics program. *Comput. Phys. Commun.* 62:187–197.
28. Chang, C. E., T. Shen, J. Trylska, V. Tozzini, and J. A. McCammon. 2006. Gated binding of ligands to HIV-1 protease: Brownian dynamics simulations in a coarse-grained model. *Biophys. J.* 90:3880–3885.
29. Chang, C. E. A., J. Trylska, V. Tozzini, and J. A. McCammon. 2007. Binding pathways of ligands to HIV-1 protease: coarse-grained and atomistic simulations. *Chem. Biol. Drug Des.* 69:5–13.
30. Trylska, J., V. Tozzini, C. E. Chang, and J. A. McCammon. 2007. HIV-1 protease substrate binding and product release pathways explored with coarse-grained molecular dynamics. *Biophys. J.* 92:4179–4187.
31. Trylska, J., V. Tozzini, and J. A. McCammon. 2005. Exploring global motions and correlations in the ribosome. *Biophys. J.* 89:1455–1463.
32. Ermak, D. L., and J. A. McCammon. 1978. Brownian dynamics with hydrodynamic interactions. *J. Chem. Phys.* 69:1352–1360.
33. Shen, T. Y., C. F. Wong, and J. A. McCammon. 2001. Atomistic Brownian dynamics simulation of peptide phosphorylation. *J. Am. Chem. Soc.* 123:9107–9111.
34. Cheng, X., B. Lu, B. Grant, R. J. Law, and J. A. McCammon. 2006. Channel opening motion of alpha7 nicotinic acetylcholine receptor as suggested by normal mode analysis. *J. Mol. Biol.* 355:310–324.
35. Grant, B. J., A. P. Rodrigues, K. M. ElSawy, J. A. McCammon, and L. S. Caves. 2006. Bio3d: an R package for the comparative analysis of protein structures. *Bioinformatics.* 22:2695–2696.
36. Brooks, B. R., R. E. Bruccoleri, B. D. Olafson, D. J. States, S. Swaminathan, and M. Karplus. 1983. CHARMM—a program for macromolecular energy, minimization, and dynamics calculations. *J. Comput. Chem.* 4:187–217.
37. McCammon, J. A., and S. H. Northrup. 1981. Gated binding of ligands to proteins. *Nature.* 293:316–317.
38. Szabo, A., D. Shoup, S. H. Northrup, and J. A. McCammon. 1982. Stochastically gated diffusion-influenced reactions. *J. Chem. Phys.* 77: 4484–4493.
39. Fetrow, J. S. 1995. Omega loops: nonregular secondary structures significant in protein function and stability. *FASEB J.* 9:708–717.
40. Boyd, A. E., C. S. Dunlop, L. Wong, Z. Radic, P. Taylor, and D. A. Johnson. 2004. Nanosecond dynamics of acetylcholinesterase near the active center gorge. *J. Biol. Chem.* 279:26612–26618.
41. Bourne, Y., Z. Radic, H. C. Kolb, K. B. Sharpless, P. Taylor, and P. Marchot. 2005. Structural insights into conformational flexibility at the peripheral site and within the active center gorge of AChE. *Chem. Biol. Interact.* 157–158:159–165.
42. Taylor, P., and S. Lappi. 1975. Interaction of fluorescence probes with acetylcholinesterase. The site and specificity of propidium binding. *Biochemistry.* 14:1989–1997.
43. Bourne, Y., P. Taylor, and P. Marchot. 1995. Acetylcholinesterase inhibition by fasciculin: crystal structure of the complex. *Cell.* 83:503–512.
44. Boyd, A. E., A. B. Marnett, L. Wong, and P. Taylor. 2000. Probing the active center gorge of acetylcholinesterase by fluorophores linked to substituted cysteines. *J. Biol. Chem.* 275:22401–22408.
45. Kryger, G., M. Harel, K. Giles, L. Toker, B. Velan, A. Lazar, C. Kronman, D. Barak, N. Ariel, A. Shafferman, I. Silman, and J. L. Sussman. 2000. Structures of recombinant native and E202Q mutant human acetylcholinesterase complexed with the snake-venom toxin fasciculin-II. *Acta Crystallogr.* 56:1385–1394.
46. Harel, M., G. Kryger, T. L. Rosenberry, W. D. Mallender, T. Lewis, R. J. Fletcher, J. M. Guss, I. Silman, and J. L. Sussman. 2000. Three-dimensional structures of Drosophila melanogaster acetylcholinesterase and of its complexes with two potent inhibitors. *Protein Sci.* 9:1063–1072.
47. Harel, M., G. J. Kleywegt, R. B. Ravelli, I. Silman, and J. L. Sussman. 1995. Crystal structure of an acetylcholinesterase-fasciculin complex: interaction of a three-fingered toxin from snake venom with its target. *Structure.* 3:1355–1366.
48. Radic, Z., N. A. Pickering, D. C. Vellom, S. Camp, and P. Taylor. 1993. Three distinct domains in the cholinesterase molecule confer selectivity for acetyl- and butyrylcholinesterase inhibitors. *Biochemistry.* 32:12074–12084.
49. Saxena, A., R. S. Hur, C. Luo, and B. P. Doctor. 2003. Natural monomeric form of fetal bovine serum acetylcholinesterase lacks the C-terminal tetramerization domain. *Biochemistry.* 42:15292–15299.
50. Kairys, V., M. X. Fernandes, and M. K. Gilson. 2006. Screening drug-like compounds by docking to homology models: a systematic study. *J. Chem. Inf. Model.* 46:365–379.
51. Kairys, V., and M. K. Gilson. 2002. Enhanced docking with the mining minima optimizer: acceleration and side-chain flexibility. *J. Comput. Chem.* 23:1656–1670.